



CD7 protein plays a crucial role in T cell infiltration in tumors

Binjie Sheng^{a,b}, Kailu Zhang^a, Shuaiyu Tian^a, Renyuxue Ma^a, Zixuan Li^d,
 Hai Wu^{a,b}, Tian Wang^{a,b}, Licui Jiang^{a,b}, Fengtao You^b, Gangli An^a, Huimin Meng^b,
 Lin Yang^{a,b,*}, Xin Liu^{c,**}

^a Cyrus Tang Hematology Center, Collaborative Innovation Center of Hematology, State Key Laboratory of Radiation Medicine and Protection, Soochow University, Suzhou 215123, China

^b PersonGen BioTherapeutics (Suzhou) Co., Ltd., PR China

^c The First Affiliated Hospital of USTC, Division of Life Sciences and Medicine, University of Science and Technology of China, Hefei, Anhui, 230001, China

^d Affiliated Children's Hospital of Jiangnan University (Wuxi Children's Hospital), Wuxi, Jiangsu, 214000, China

ARTICLE INFO

Keywords:

CD7
 Hematopoietic system
 CD8⁺ T cells
 Lymphoma
 Infiltration

ABSTRACT

CD7 protein as a target is being used to treat CD7⁺ lymphoma; however, the role of CD7 in the hematopoietic system remains largely unknown. Therefore, we evaluated the effects of CD7 KO in mice. The differentiation of the hematopoietic system in the bone marrow and the number of various cell types in the thymus and spleen did not differ between CD7 KO and WT mice. After subcutaneous inoculation of B16-F10 melanoma cells, tumors from CD7 KO mice grew more rapidly, and the proportion of CD8⁺ T cells in the spleen and tumors decreased. *In vitro*, the infiltration and adhesion of CD8⁺ T cells from the spleen of CD7 KO mice were weakened. Blocking CD7 in normal T cells did not alter the migration and infiltration, but in Jurkat, CCRF-CEM, and KG-1a tumor cell lines, migration and invasion were significantly reduced after blocking CD7. Therefore, CD7 does not affect hematopoietic system development but plays a crucial role in T cell infiltration into tumors.

1. Introduction

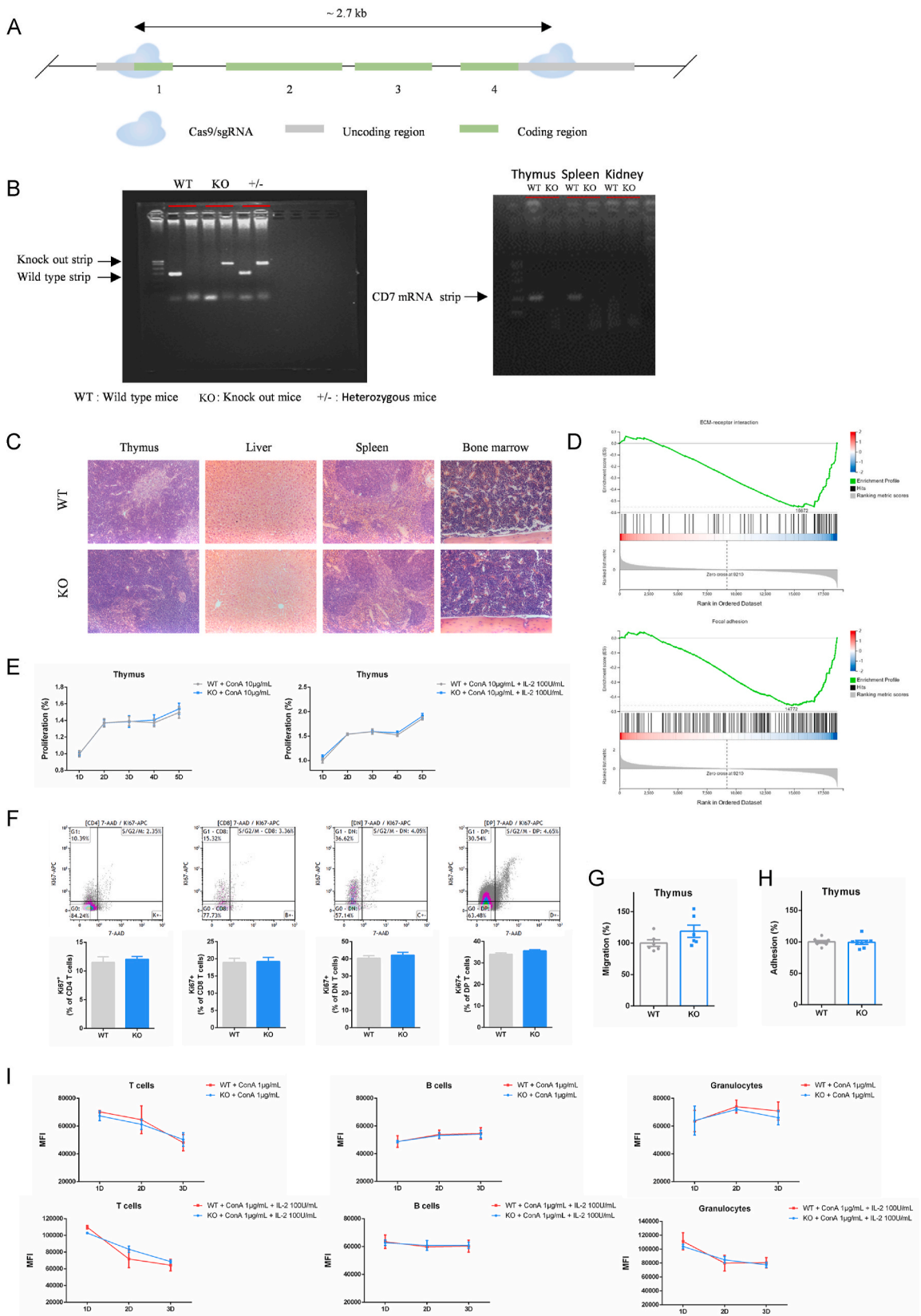
CD7, also known as GP40, is a membrane-expressed protein that belongs to the immunoglobulin superfamily. CD7 expression was detected in T cells and subsequently shown to also be present on natural killer (NK) cells [1–3], indicating a role for CD7 in the immune system. In addition, CD7 is highly expressed in patients with T-acute lymphoblastic leukemia (T-ALL), T cell lymphoblastic lymphoma (T-LBL), and acute myeloid leukemia (AML) and is closely related to the occurrence and development of most T cell derived malignancies [4–6]. More CD7 expression is also associated with poor prognosis in patients with acute lymphoblastic leukemia [7,8].

CD7 has been extensively examined *in vitro*. CD7 has two ligands, K12 protein and galectin-1 [9,10]. K12 is regulated by IFN- γ [11], and a combination of K12 and CD28 antibodies can promote the proliferation of human T cells [12]. Binding to K12 to NK cells increases CD25 and CD69 expression in these cells [2]. Additionally, K12 can increase the migration ability of monocytes after binding to

* Corresponding author. No.199 Ren'ai Road, Suzhou Industrial Park, Jiangsu Province, 215123, China.

** Corresponding author. Department of Hematology, First Affiliated Hospital of University of Science and Technology of China (Anhui Provincial Hospital), No.17 Lujiang Road, Luyang District, Hefei City, Anhui Province, 230001, China.;

E-mail addresses: yanglin@suda.edu.cn (L. Yang), lxinahf@163.com (X. Liu).



(caption on next page)

Fig. 1. CD7 gene KO mice and cell function test. (A) Schematic diagram of the construction of CD7 KO mice. (B) CD7 knockout mice genotype identification, DNA level identification (left), RNA level identification (right). (C) H&E staining of mice thymus, liver, spleen, and bone marrow, eyepiece \times objective = 10×20 . (D) Comparison of WT mice thymocytes with CD7 KO mice thymocytes by gene set enrichment analysis (enrichment map of ECM interaction and focal adhesion pathway). Red and blue represent high and low gene expression, respectively ($n = 3$). (E) Detection of the proliferation ability of mice thymocytes treated with $10 \mu\text{g/mL}$ Con A or $10 \mu\text{g/mL}$ Con A + 100 U/mL , using CCK-8 to detect the absorbance at OD450 nm ($n = 3$). (F) Detection of Ki67 levels of DN, DP, CD4^+ , and CD8^+ T cells in mice thymus ($n = 6$). (G–H) Detection of mice thymus migration ability (G) and adhesion ability (H) under normal physiological conditions. Migration (%) and adhesion (%) were calculated based on the average of the migration and adhesion level of WT mice thymocytes as 100% ($n = 6$). (I) Detection of the proliferation ability of mice spleen T cells, B cells, and granulocytes; mean fluorescence intensity (MFI) of CFSE for three consecutive days after spleen cells were isolated ($n = 3$). Statistical analysis of WT mice vs. CD7 KO mice NS, not significant. (For interpretation of the references to colour in this figure legend, the reader is referred to the Web version of this article.)

CD7 [13]. The binding of galectin-1 to CD7 promotes T cell apoptosis [14–16]. In addition, many researchers have attempted to use CD7-monoal antibodies (mAbs) to activate CD7. Rabinowich et al. reported that binding to CD7mAb increased the adhesion of NK cells to fibronectin [17]. For T cells, binding to CD7mAb not only increased their adhesion but also increased T cell intracellular calcium ion concentration and the proliferative ability of both γ/δ T and α/β T cells [18–22]. Previous studies showed that CD7 plays a vital role in T and NK cell functions after binding to its ligands and antibodies. However, the role of CD7 under normal physiological conditions remains unclear.

Compared with human CD7, mice CD7 lacks four proline-rich repetitive sequences in its extracellular domain [23]. Because the extracellular domain is shorter than in humans, no anti-mouse CD7 antibody is available. The *in vivo* role of CD7 has been evaluated in numerous studies [24–27]. Lee et al. revealed a significant increase in the number of thymic double-positive T cells in 3-month-old CD7 KO mice. Following stimulation with tetanus toxin, the expression level of IFN- γ in the thymocytes and MHC I-restricted cytotoxic T lymphocyte activity in CD7 KO mice decreased [24]. Additionally, Bonilla et al. reported that deletion of the CD7 gene did not affect the thymocyte type and proportion of B cells, T cells, and NK cells in the spleen of 10-month-old mice [25]. Under LPS-induced conditions, CD7 KO mice could tolerate LPS-mediated shock, which was explained by the lower proportion of natural killer T (NKT) lymphocytes in the liver of CD7 KO mice [26]. However, the effect of CD7 in mice and whether CD7 impacts the development of the entire hematopoietic system have not been determined.

In the field of lymphoma treatment, adoptive immunotherapy, led by CAR-T cell therapy, is applied worldwide [28–30]. In CD7-CAR-T therapy, not only the CD7 of CAR-T cells is blocked or knocked out, After CD7-CAR-T treatment, the patients themselves also lost CD7. However, the effects of the loss of CD7 molecules in cells are unclear; thus, studies of the function of CD7 are particularly important.

We examined the effect of CD7 KO on the entire hematopoietic system of mice. The development process of T cells in the thymus and the proportion of various types of cells in the spleen were evaluated to determine the effect of the CD7 on murine immune system development. Additionally, the infiltration and adhesion of CD8^+ T cells in the spleen of CD7 KO mice with tumors and the effects on tumor growth were examined. Our results indicate that CD7 loss is not affecting the development of hematopoietic system and suggest that we should deal with the possible weakening of T cells infiltration capacity after CD7-targeted lymphoma therapy.

2. Results

2.1. Construction of CD7 gene KO mice and functional verification

To examine the role of CD7 in normal cells, we used CRISPR/Cas9 technology to construct CD7 KO mice (Fig. 1A and B). Assessment of the overall structure, cell composition, and cell morphology of murine thymus, liver, spleen, and bone marrow by pathologists revealed no significant difference compared with WT mice (Fig. 1C). In addition, there were also no differences in the organ weights and cell numbers of mice compared with WT mice (Supplemental Fig. 1A). To further explore the effects of the loss of CD7, we performed RNA-sequencing of murine thymocytes and NK cells. NK cells in the bone marrow showed fewer differentially expressed genes compared to thymocytes, and thus we focused on T cells in subsequent analysis (Supplemental Fig. 1B 1C). To evaluate mice thymocytes, we performed Gene Set Enrichment Analysis (GSEA). Results showed that the lack of CD7 may affect the interaction of mice thymocytes with the extracellular matrix and focal adhesion (Fig. 1D). Based on these results, we analyzed the function of mice thymocytes by detecting their proliferation, migration, and adhesion. CD7 KO mice thymocytes showed no difference in their expansion ability compared with WT mice after stimulation with concanavalin A (Con A) and Con A + IL-2 *in vitro* (Fig. 1E). In addition, compared with WT mice, Ki67 levels in mice thymus double-negative (DN), double-positive (DP), CD4^+ , and CD8^+ T cells did not differ (Fig. 1F). *In vitro* CD7 KO mice and WT mice thymocytes displayed comparable migration and adhesion abilities (Fig. 1G and H). RNA-sequencing showed that CD36 expression in the thymocytes of CD7 KO mice was weakened. Thus, we tested CD36 expression in mice thymus DN, DP, CD4^+ , and CD8^+ T cells. The expression level of CD36 in CD4^+ T cells of CD7 KO mice was indeed reduced by 40.0% compared with WT mice (Supplemental Fig. 1D). We also evaluated the expansion ability of mice spleens T, B, and granulocytes *in vitro*. After ConA and Con A + IL-2 stimulation *in vitro*, T and granulocytes expanded, but there was no difference in expansion ability between KO and WT mice (Fig. 1I). Together, our results suggest that under normal physiological conditions, a lack of CD7 does not affect the growth and development of mice or cell functions.

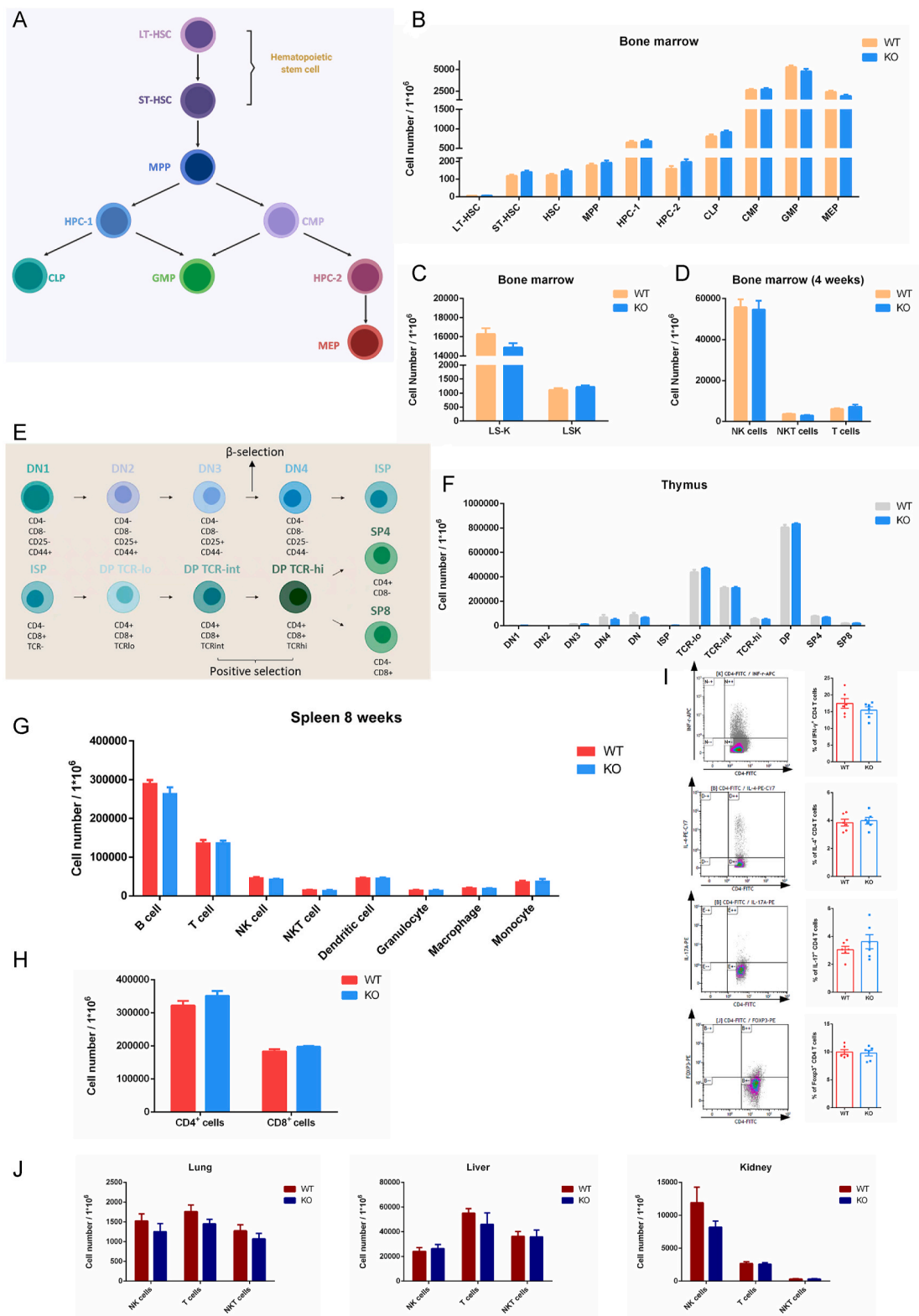


Fig. 2. CD7 KO mice organ cells did not change under normal physiological conditions. (A) Schematic diagram of mice hematopoietic system differentiation. (B–D) Statistics of each cell type of the hematopoietic system in the bone marrow of 8-week-old WT mice and CD7 KO mice, represented by the corresponding number of cells per million bone marrow cells ($n = 12$). (E) Schematic diagram of T cell development in the mice thymus. (F) Statistics of cell types in the thymus of 8-week-old WT mice and CD7 KO mice, represented by the corresponding number of cells per million thymocytes ($n = 12$). (G) Statistics of cell types in 8-week-old WT mice and CD7 KO small spleen, represented by the corresponding number

of cells per million spleen cells ($n = 12$). (H) $CD4^+$ T cells and $CD8^+$ T cells are represented by the number of corresponding cells per million spleen cells ($n = 6$). (I) Expressed as the percentage of Th1, Th2, Th17, and Treg cells in $CD4^+$ T cells ($n = 6$). (J) Under normal physiological conditions, NK, NKT, and T cell numbers. Statistical analysis of WT mice vs. CD7 KO mice; NS, not significant.

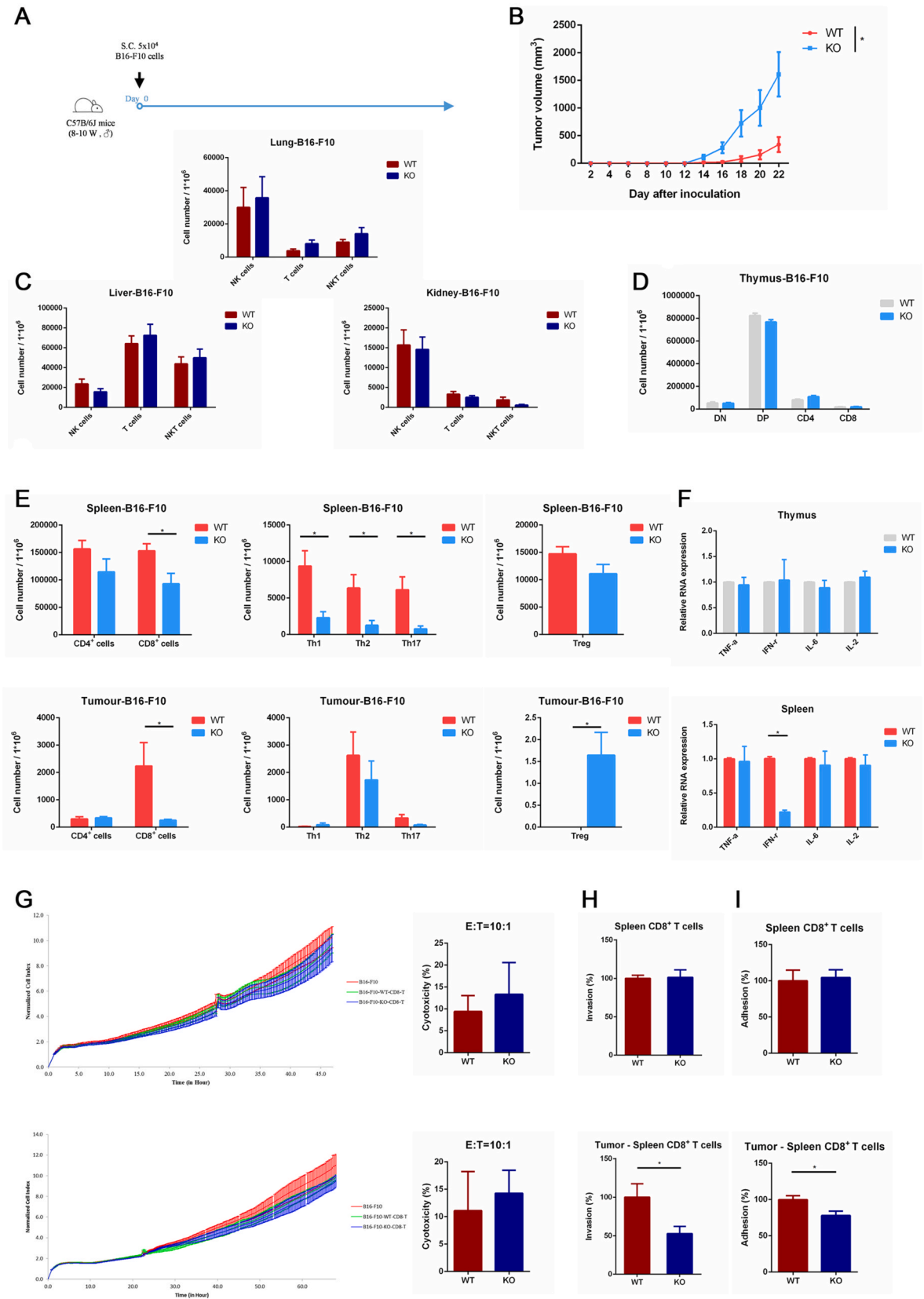
2.2. Detection of the hematopoietic system in CD7 KO mice

As CD7 is highly expressed on T cells and NK cells, we examined whether a lack of CD7 impacts the murine hematopoietic system (Fig. 2A). First, we detected hematopoietic stem cells in the bone marrow. We found no significant difference in $Lin^-Sca1^+Kit^+$ (LSK), $Lin^-Sca1-Kit^+$ (LS-K), hematopoietic stem cell (HSC), multipotent progenitor (MPP), hematopoietic progenitor cells-1 (HPC-1), hematopoietic progenitor cells-2 (HPC-2), common lymphoid progenitors (CLP), common myeloid progenitors (CMP), granulocyte-macrophage progenitor (GMP), megakaryocyte-erythrocyte progenitor (MEP), NK, NKT, or T cells in the bone marrow of 8-week-old mice between KO and WT mice (Fig. 2B–D). In previously reported, CD7 KO mice showed increased thymic DP cells at 3 months old, and thus we also tested 4- and 12-week-old mice. The detection of hematopoietic stem cells in the bone marrow of 4- and 12-week-old mice yielded the same results, with no significant difference (Supplemental Figs. 2A–D). We then tested the entire developmental process of T cells in the murine thymus (Fig. 2E). For DN1, DN2, DN3, DN4, immature single-positive (ISP), DP, CD4 single-positive (SP4), and CD8 single-positive (SP8) cells in the thymus of 8-week-old mice, no significant differences were found between KO and WT mice (Fig. 2F). Similar results were observed in the thymus of 4- and 12-week-old mice (Supplemental Figs. 2E–F). Next, we examined spleen cells, compared with WT mice, CD7 KO mice with no significant difference found in B cells, T cells, NK cells, NKT cells, dendritic cells, granulocytes, monocytes, macrophages, $CD4^+$ T, $CD8^+$ T, Th1, Th2, Th17, and Treg cells in the spleen of 8-week-old mice (Fig. 2G–I). There were also no significant differences in the spleen cells of the mice at 4 and 12 weeks of age between KO and WT mice (Supplemental Fig. 2G–H). In addition, the $CD4^+$ T, $CD8^+$ T, and Treg cells of CD7 KO mice and WT mice showed comparable expression levels of CD36 (Supplemental Fig. 2I). Then, we analyzed NK, NKT, and T cells infiltration in the lung, liver, and kidney of 8-week-old mice and found no variation between KO and WT mice (Fig. 2J). Finally, we tested the peripheral blood cells of 8-week-old mice and also found no variation between KO and WT mice (Supplemental Fig. 3A). Altogether, these results reveal a lack of CD7 under normal physiological conditions does not affect hematopoietic system development in mice.

2.3. $CD8^+$ T cell infiltration capacity in the spleen of CD7 KO mice is weakened after tumor inoculation

The above results show under normal physiological conditions, CD7 does not exhibit the corresponding function *in vitro* and *in vivo*, so to probe the function of CD7 protein, we activated the immune system of the mice via external stimuli. We subcutaneously injected B16–F10 cells into mice (Fig. 3A). Unexpectedly, the tumors of CD7 KO mice grew faster, and WT mice showed a longer survival period (Fig. 3B) (Supplemental Fig. 3B). To explore the reasons for this variation, we analyzed the infiltration of NK, NKT, and T cells in the lungs, livers, and kidneys of mice, which showed no difference between KO and WT mice (Fig. 3C). Similar to the normal physiological conditions, the detection of DN, DP, $CD4^+$, and $CD8^+$ T cells in the CD7 KO mice thymus showed no differences compared with WT mice (Fig. 3D). Additionally, unlike normal physiological conditions, the DN, DP, $CD4^+$, and $CD8^+$ T cells of KO and WT mice detected the same CD36 protein expression levels (Supplemental Fig. 3E). Compared with WT mice, the spleens of CD7 KO mice were enlarged, and thus we further evaluated the spleen cells of the mice (Supplemental Fig. 3C). $CD8^+$ T cells in the spleen of CD7 KO mice decreased by 39.3%, and Th1, Th2, and Th17 cells also decreased significantly compared with WT mice (Fig. 3E). Tumor detection showed $CD8^+$ T cells in the tumors of CD7 KO mice decreased by 88.6%, and the proportion of Treg cells increased compared with WT mice (Fig. 3E). This also explains why tumors grew more rapidly in CD7 gene KO mice. In addition, the CD36 expression level was decreased in $CD8^+$ T cells in the spleen but not in the tumor (Supplemental Fig. 3F).

We extracted cells from the thymus and spleen to detect the expression of cytokine mRNA and observed that $IFN-\gamma$ mRNA expression decreased by 81.5% in the spleen of CD7 KO mice subcutaneously injected B16–F10 cells, compared with WT mice (Fig. 3F). This may be because of the release reduction of $IFN-\gamma$ of $CD8^+$ T cells in the spleen of these mice (Supplemental Fig. 6B). According to the results of our previous GSEA, we guessed whether, after injection of B16–F10 cells, the infiltration and adhesion were weakened in $CD8^+$ T cells in CD7 KO mice, resulting in fewer cells entering the tumor. Therefore, we sorted the mice spleen $CD8^+$ T cells for *in vitro* analysis after subcutaneously injected B16–F10 cells or PBS. First, regardless of whether tumors were injected, the $CD8^+$ T cells of the spleen between KO and WT mice demonstrate the same inhibitory ability on B16–F10 cells (Fig. 3G). Moreover, there was no difference in the chemotaxis ability of $CD8^+$ T cells of CD7 KO mice *in vitro* (Supplemental Fig. 3H) or the level of Ki67 in $CD8^+$ T cells of CD7 KO mice after tumors were injected, compared with WT mice (Supplemental Fig. 3G). Finally, the infiltration and adhesion of $CD8^+$ T cells in the spleen of CD7 KO mice was reduced by 56.0% and 34.9%, respectively, after tumors were injected, compared with WT mice. In contrast, these phenomena were not observed in mice under normal physiological conditions (Fig. 3H and I). Thus, under normal physiological conditions, CD7 does not perform the corresponding function; however, in the presence of external inducing factors, such as tumor inoculation, CD7 increases the infiltration and adhesion of $CD8^+$ T cells in the spleen of mice. Finally, for humoral immunity, the same proportion of IgG antibodies that specifically recognize B16–F10 were detected in the peripheral blood plasma of KO and WT mice three weeks after tumor inoculation (Supplemental Fig. 3D). Due to the enlarged spleen of CD7 KO mice, red blood cells, platelets, and hematocrit in the peripheral blood of CD7 KO mice were reduced, compared with WT mice (Supplemental Fig. 3I). Hence, based on these results, CD7 mainly functions to increase the infiltration capacity of $CD8^+$ T cells in the presence of tumors.



(caption on next page)

Fig. 3. The presence of tumors enables CD7 to enhance the infiltration capacity of CD8⁺ T cells in the spleen of mice. (A) C57BL/6J mice were inoculated subcutaneously with 5×10^4 B16–F10 mice melanoma cells. (B) Tumor growth detection (n = 6). (C) After tumor inoculation, when the tumor of CD7 KO mice reached 1000 mm³, the lungs, livers, and kidneys of WT mice and CD7 KO mice were collected to evaluate infiltration of NK, NKT, and T cells (n = 6). (D) Number of DN, DP, CD4, and CD8 cells per million thymocytes (n = 6). (E) CD4⁺ T cells and CD8⁺ T cells in the mice spleen and tumors are represented by the corresponding number of cells per million spleen cells (n = 6), Th1, Th2, Th17, and Treg cells accounted for the percentage of CD4⁺ T cells (n = 6). (F) When the tumor of CD7 KO mice reached 1000 mm³, total RNA was extracted from the thymus and spleen of WT mice and CD7 KO mice. The mRNA level of a specific cytokine is reported as a percentage of the GAPDH signal. The data represent the mean \pm SEM of the results obtained from three mice. (G) Killing ability of sorted spleen CD8⁺ T cells against B16–F10 cells *in vitro*. E: T (effective: target) = 10:1, real-time cell index detection using real-time cell analysis instrument. Killing ability was defined as the ability to inhibit the cell index of B16–F10 cells (n = 6). (H–I) Adhesion capacity of sorted spleen CD8⁺ T cells *in vitro* and infiltration capacity of B16–F10 cells. The infiltration and adhesion capacity of CD8⁺ T cells in the spleen of WT mice was defined as 100% and used to statistically analyze CD7 KO mice (n = 6). *P < 0.05.

2.4. Blocking CD7 did not affect T cell functions in the peripheral blood of normal individuals

To verify these results in human T cells, we blocked CD7 expression in peripheral blood T cells from three normal donors using the protein expression blocker (PEBL) (Fig. 4A). We first detected the expression of the common and activated markers CD3, CD4, CD8, CD7, CD25, CD69 and CD45 on the surface of T cells, which revealed no abnormal expression after blocking CD7 (Fig. 4B). No significant difference was found in the antigen densities of CD3 and CD45 between T and T-CD7-PEBL cells (Supplemental Fig. 4A). Approximately 10% of T cells in the peripheral blood of normal subjects were CD7-negative T cells. Phenotypic testing showed that most of these cells were effector memory cells; in CD7-blocked T cells, the lack of CD7 did not affect the T cell phenotype. Therefore, CD7-negative T cells and CD7-blocked T cells in the peripheral blood of normal subjects were not the same types of cells (Supplemental Fig. 4B).

We next constructed CD276-CAR-T cells to detect the tumor suppressor ability after the loss of CD7. The tumor suppressor ability of CD276-CAR-T cells after blocking CD7 *in vitro* was not affected compared with T cells (Fig. 4C). Moreover, for T cells from the three normal donors, the presence or absence of CD7 did not affect the apoptosis and cell cycle of T cells. The migration ability, infiltration ability, chemotaxis ability to tumor cells, and adhesion ability of T cells showed the same result, with no difference (Fig. 4D–I), implying that CD7 does not perform the corresponding function under normal physiological conditions. Finally, for the three normal donors, no large differences were found in migration- and adhesion-related genes (Supplemental Fig. 4C). The above results indicate that similar to mice, in human peripheral blood, CD7 does not affect the infiltration and adhesion of T cells under normal physiological conditions.

2.5. CD7 affects the ability of tumor cells to metastasize

Because CD7 is also expressed on T-ALL and AML tumor cells, we examined whether CD7 expression in cell lines is the same as CD7 in human peripheral blood T cells and if it plays any significant role. We blocked CD7 in Jurkat, CCRF-CEM, and KG-1a cells through PEBL (Supplemental Fig. 5A). Consistent with human peripheral blood T cells, no abnormal expression of CD3, CD4, CD8, CD25, CD69, CD34, CD45, and PD-1 was observed on the surface of the three cell lines after blocking CD7 (Supplemental Fig. 5B). In the cell cycle, the proportion of G0 and G1 phase cells in the three cell lines slightly increased after blocking CD7 (Fig. 5A). Apoptosis of Jurkat and CCRF-CEM cells increased slightly after blocking CD7, whereas cell viability was not affected (Fig. 5B). In addition, there was no difference in PD-1 expression on the T cell surface after T cells were separately co-incubated with Jurkat-GFP and Jurkat-CD7-PEBL (Supplemental Fig. 5C). Thus, blocking of CD7 had no obvious effect on the cell apoptosis, cell cycle, or T cell response.

We next tested the migration, adhesion capabilities of the three cell lines, which revealed significant decreases after blocking CD7 (Fig. 5C and D). The invasion capabilities of Jurkat and CCRF-CEM cells decreased significantly after blocking CD7 (Fig. 5E). Finally, analysis of the expression of migration- and adhesion-related genes in the three cell lines showed that ITGB1 and ITGB3 were significantly downregulated (Supplemental Fig. 5D). The antigen density of ITGB1 on the cell surface was decreased, ITGB3 expression on the surface of KG-1a-CD7-PEBL cells decreased after CD7 was blocked (Supplemental Fig. 5E). These results indicate that blocking of CD7 impacts tumor cells migration, invasion, and adhesion, and thus may affect tumor metastasis.

Jurkat-GFP and Jurkat-CD7-PEBL cells were injected into NCG mice through the tail vein; NCG mice injected with Jurkat-GFP and Jurkat-CD7-PEBL cells had the same survival time and body weight change. Furthermore, the peripheral blood tumor burden test showed no difference (Fig. 5F–H). The mice were sacrificed 4 weeks after tumor inoculation, and tumor infiltration in various organs was evaluated. Compared with mice injected with Jurkat-GFP cells, the proportion of tumor cells of the mice injected with Jurkat-CD7-PEBL cells in the liver was higher, and the proportion in the bone marrow was lower. Changes in the expression of chemokine receptors and integrins after CD7 blockade may be responsible for the metastasis of Jurkat cells to different organs (Supplemental Fig. 5D, 5E).

3. Discussion

As a target for treating lymphoma, CD7 has attracted increasing attention. However, the functional understanding of CD7 remains limited. We aimed to explore the role of CD7 and evaluated the effect of CD7 loss on the hematopoietic system.

The lack of CD7 did not affect hematopoietic system development in mice. In CD7 KO mice, the tissue structure and cell number of murine immune organs were unaffected. The hematopoietic system development in the bone marrow of CD7 KO mice, T cell

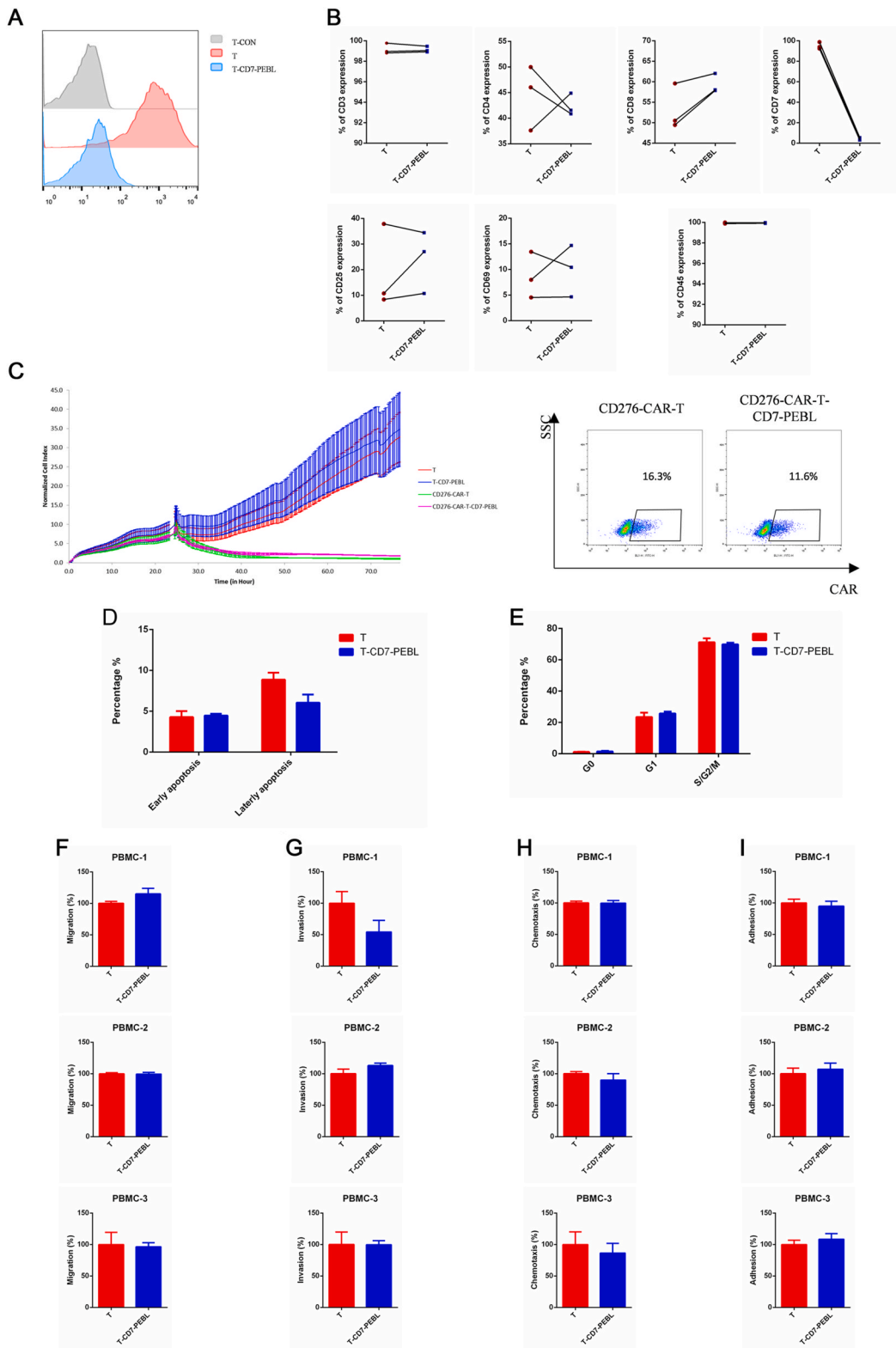


Fig. 4. CD7 protein in normal donor peripheral blood T cells. (A) After blocking CD7, the expression of CD7 on the surface of peripheral blood T cells. (B) Expression of CD3, CD4, CD8, CD7, CD25, CD69, and CD45 on the peripheral blood T cells and T-CD7-PEBL cells of normal donors (n = 3). (C) Three generations of CD276-CAR-T cells were constructed based on T cells and T-CD7-PEBL cells. The ability of CD276-CAR-T cells to kill the SW1990 pancreatic cancer cell line *in vitro*, E: T (effective: target) = 1:1 (Left). Positive rate of CD276-CAR-T cell construction (right). (D–E) T cell

and T-CD7-PEBL cell apoptosis (D) and cell cycle (E). Results are expressed as a percentage of the total number of cells ($n = 3$). (F–I) Migration, infiltration, chemotaxis, and adhesion of T cells in the peripheral blood of three normal donors. Using T cells as the standard, changes after blocking CD7 were evaluated for T cells and vs. T-CD7-PEBL cells; NS, not significant.

development in the thymus, and proportion of cells in the spleen were not affected by CD7 deletion. Most previous studies of CD7 KO mice revealed no T cell development- and function-related abnormalities [25,27]. Unlike the results found by Lee et al. [24], we did not observe a difference in the number of cells in the thymus of 3-month-old mice. This may be because of a higher number of mice included in the study, thereby creating a more reliable result. Kim et al. reported that human CD34⁺ cells in which the CRISPR/Cas9 was used to knock out CD7 showed the same proportion of myeloid and lymphoid lineages as normal CD34⁺ cells in NSGS mice [31], and signs of T cell maturation were observed in a CD7-deficient patient [32]. Therefore, CD7 KO mice developed a complete CD7-negative hematopoietic system.

Under normal physiological conditions, the loss of CD7 does not affect the migration and adhesion of T cells. As the GSEA showed a weakening trend in the interaction between CD7 KO mice thymocytes and the extracellular matrix, we analyzed the function of mice thymocytes. However, we did not detect the decrease in the ability of CD7 KO mice thymocytes to adhere to Matrigel *in vitro*, compared to WT mice; this may be because, under normal physiological conditions, such differences are subtle and not significant, so they cannot be detected *in vitro*. In addition, compared to normal human peripheral blood T cells, there was no difference in terms of migration, infiltration, and adhesion ability in CD7 KO cells, providing further experimental support. Previous studies demonstrated no difference in the killing function of NK cells in CD7 gene-deficient mice compared with WT mice [24]. There was also no difference between the killing ability and cytokine production ability of CAR-T cells in which CD7 was blocked or knocked out compared with normal T cells [30]. Therefore, under normal physiological conditions, although CD7 is expressed on the membrane surface, CD7 may not participate in the physiological functions of cells.

In the presence of tumors, CD7 upregulates the infiltration capacity of CD8⁺ T cells. Numerous studies have reported that CD7 affects the adhesion to fibronectin of NK and T cells after CD7 mAb-mediated activation [33–36]. We found that, under normal physiological conditions, the invasion and adhesion capabilities of CD8⁺ T cells in the mice spleen *in vitro* did not significantly differ between KO and WT mice. However, in the presence of tumors, the invasion and adhesion capabilities of CD8⁺ T cells in the spleen of CD7 KO mice *in vitro* were significantly reduced compared with WT mice. Based on these results, we speculate that in the presence of tumors, the infiltration capacity of CD8⁺ T cells in CD7 KO mice was weakened, resulting in fewer CD8⁺ T cells entering the tumor and causing the tumor to grow more rapidly. CD7 may require stimuli such as ligands to exert its function. CD7 is inactive under normal physiological conditions.

High expression of CD7 in lymphoma can increase the metastatic ability of tumor cells. The main functional varieties of tumor cells after CD7 blocking are reflected in their migration, adhesion, and invasion abilities. Both normal human peripheral blood T cells and T lymphoma cells have CD7 expression on the membrane surface, but unlike normal human peripheral blood T cells, the invasion and adhesion ability of T lymphoma cells is weakened after blocking CD7. Previous studies by Kondoh et al. also showed that CD7 expression levels positively correlated with the migration ability of B cell acute lymphoblastic leukemia cells [19]. CD7 increases the ability of tumor cells to metastasize, explaining how CD7 expression is related to patient prognosis. However, it is unclear whether the effect of CD7 on tumor cell metastasis is due to the higher CD7 antigen density in tumor cells or because the downstream signal pathway of CD7 is activated in tumor cells, representing a shortcoming of our research.

Notably, the increase in adhesion caused by CD7 may be related to integrins. In all three tumor cell lines, the mRNA levels of ITGB1 and ITGB3 were significantly downregulated after blocking CD7. Detection at the level also revealed ITGB1 and ITGB3 downregulation, consistently with the results of previous studies [18]. Interestingly, Fukumori et al. found that CD7 and ITGB1 co-localize [37], further explaining the interaction between CD7 and integrins. Our current study also found that CD7 is co-located with ITGB1 in three tumor cell lines, but not with ITGB3 (Supplemental Fig. 6A). Integrin enhances cell adhesion to extracellular matrix due to clustering or conformational change [38]. We hypothesized that clustering of integrins induced by CD7 may be the key to increase T cell adhesion. However, how CD7 regulates the functions of integrins requires further research.

Approximately 10% of CD7-negative T cells are present in the peripheral blood T cells of normal individuals [3]. Most CD7-negative T cells were effector memory cells. Moreover, CD7 expression in CD4⁺ naïve T cells is reportedly two-fold higher than that in CD4⁺ memory cells [18]. However, compared to peripheral blood T cells from normal donors, blocking CD7 did not alter the phenotype of T cells, suggesting that CD7 is not a crucial factor causing phenotypic changes in these cells. CD7 expression in T cells may be required only at a certain stage.

According to our results, there may be an association between CD3 and CD7. After CD7 was blocked in normal donor peripheral T cells, the antigen density of CD3 protein on the cell surface was downregulated in the cells from all three normal donors. In addition, previous studies showed that CD3 antibodies increased the expression of CD7 mRNA after T cells stimulation, although this effect was not observed for tumor cells [39,40]. Following stimulation of CD3 and CD28, CD7 expression levels in T cells increased [16]. According to Lazarovits et al. CD7 is part of an oligomeric complex formed by CD3/TCR and CD45 [41].

Additionally, CD7 may be related to the IFN- γ release. Lee et al. found that the release of IFN- γ from thymocytes in CD7 KO mice was weakened by stimulation with tetanus toxin compared with WT mice [24]. Subsequently, they found that the mRNA level of IFN- γ in the liver cells of CD7 KO mice was reduced after induction with LPS compared with WT mice [26]. In our study, the mRNA level of IFN- γ in the spleen cells of CD7 KO mice decreased in the presence of tumors; however, this effect was not observed in the thymus. Other studies reported that CD7 mAb increases the release of IFN- γ from NK cells *in vitro* [17], although there are no reports on abnormal IFN- γ release from CAR-T cells after CD7 is knocked out [3].

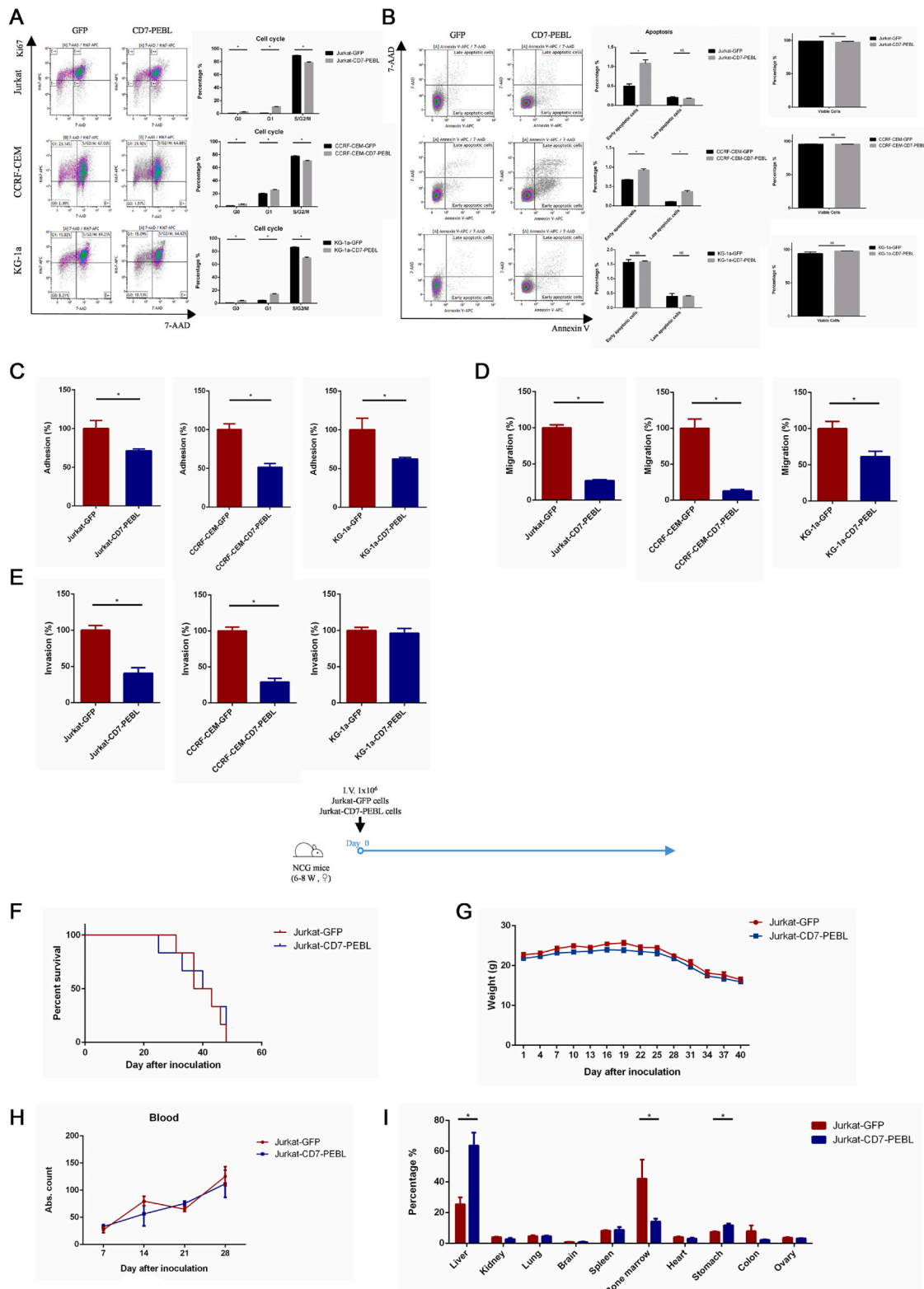


Fig. 5. After blocking CD7 in the tumor cell line, the metastatic ability was weakened. (A–B) Comparison of cell cycle (A) and apoptosis (B) of Jurkat, CCRF-CEM, and KG-1a cells after blocking CD7 and corresponding cells transfected with empty GFP ($n = 3$). The results were verified in more than three repeated experiments. (C–E) Jurkat, CCRF-CEM, and KG-1a cell adhesion, migration, and invasion ability after blocking CD7 using cells transfected with empty GFP as a standard. Blocked Jurkat, CCRF-CEM, CCRF-CEM, KG-1a cells ($n = 3$). The results were verified in more than

two repeated experiments. (F–G) After tail vein injection of 1×10^6 Jurkat-GFP or Jurkat-CD7-PEBL cells, the survival period and weight change of NCG mice ($n = 6$) were determined. (H) Blood was collected from the orbit, the tumor burden in the peripheral blood of NCG mice was evaluated. The tumor was labeled with anti-human CD45 antibody, and detection was performed for 4 weeks ($n = 6$). (I) Mice were killed after the first mice died, and tumors in the mice organs were labeled with anti-human CD45 antibody ($n = 6$). * $P < 0.05$.

Finally, we speculate that there may be an association between CD7 and PPAR signaling pathways. In the following analysis, we found that PPAR signaling pathway-related genes in both mouse and human T cells were more enriched in wild type (Supplemental Fig. 6C). It has been reported that integrin proteins can regulate PPAR- γ expression [42,43], and that attenuated PPAR- γ expression will result in decreased IFN- γ release and CD36 expression [44,45], which is consistent with our observations. PPAR- γ will be the key to discovering the regulation of CD7 signaling and the focus of our group's future work.

In conclusion, deletion of the CD7 gene did not affect the development of the murine hematopoietic system or affect mice growth. After blocking CD7, normal donor T cells did not show weakened infiltration and other abilities, further proving that targeting CD7 to treat lymphoma is a feasible option. In addition, in the presence of tumors, CD7 increases the infiltration capacity of CD8⁺ T cells, thus clarifying the limitations and the role of CD7, thereby providing a theoretical framework for evaluating the clinical response to possible side effects caused by CD7 deletion.

4. Materials and methods

4.1. Mice

C57BL/6J mice were purchased from GemPharmatech (Nanjing, China). Exons 1–4 of the CD7 transcript were selected according to the structure of the CD7 gene as the KO region. The KO region was approximately 2.7 kb and contained all coding regions to delete CD7 protein. Single-guide RNA was transcribed *in vitro*, and Cas9 and single-guide RNA were microinjected into fertilized eggs of C57BL/6J mice to obtain F0 generation mice. After PCR and sequencing, the correct F0 generation in C57BL/6J^{+/-} mice was verified. C57BL/6J^{-/-} and C57BL/6J^{+/+} mice were obtained by the mating of C57BL/6J^{+/-} mice. All experiments were performed using 8-week-old mice unless otherwise specified.

A fresh tissue sample from the mice tail was placed in 100 μ L lysis buffer (50 mM Tris, pH 10.0, 100 mM Tris-HCl 0.5% Triton X-100, and 0.2 mg/mL proteinase K), digested in a water bath at 55 °C for 4 h, and then treated in a 95 °C metal bath for 10 min to stop digestion. We use the DNA cleaved from the tail of the mice as a template to perform (Tm = 65–0.5 °C/cycle, 20 cycles, Tm = 55 °C, 20 cycles, WT-F: TTCAGTTCCTTTCAGAGCAGC, WT-R: ACTCCAGACAGCCATAGTCCTATC, KO-F: AACAGGTGAGACCACAGACCTGAAC, KO-R: AATCCCTGCCCTCTTCAGGTA) in the Taq Master Mix (vazyme, Nanjing, China) system, followed by agarose gel electrophoresis of the PCR products to detect the CD7 gene of the mice. All primers used in this article were purchased from Synbio Technologies (Suzhou, China).

Mice spleen, thymus, and liver tissues were extracted using an RNA isolation reagent kit (Omega Bio-tek, Inc., Norcross, GA, USA). To separate and purify the total RNA of mice organs. Random primers and a reverse transcription kit (Thermo Fisher Scientific, Waltham, MA, USA) were used to produce whole-genome cDNA from the RNA. We use the cDNA obtained by reverse transcription as a template to perform PCR (Tm = 65 °C, 35 cycles, WT-F: CTTGAGTTCCTTTCAGAGCAGC, WT-R: ACTCCAGACAGCCATAGTCCTATC) in the Taq Master Mix (vazyme, Nanjing, China) system, followed by agarose gel electrophoresis for detection to detect the CD7 mRNA of the mice tissues.

All animals were housed in a pathogen-free facility at Soochow University, and all experimental studies were approved and conducted in accordance with the guidelines and regulations implemented by the Soochow University Animal Welfare Regulations.

4.2. Cell lines and *in vitro* culture

Jurkat, CCRF-CEM, and KG-1a cells were obtained from ATCC (Manassas, VA, USA). Jurkat and CCRF-CEM cells were cultured in RPMI (10% FBS), and KG-1a cells were cultured in KG-1 medium (Zeye, Shanghai, China) and used in experiments after reaching the exponential growth phase. B16–F10 cells were a gift from Professor Huang Yuhui of Soochow University. These cells were cultured in DMEM (10% FBS) and used for experiments after reaching the exponential growth phase. Peripheral T cells from normal donors were cultured in TexMACs medium (Miltenyi Biotec, Gladbach Bergisch, Germany) and treated with TransAct (Miltenyi Biotec), human recombinant IL-7 (155 IU/mL) and human recombinant IL-15 (290 IU/mL) to activate. Two days later, activated T cells were used for lentiviral transduction.

To construct Jurkat-GFP, CCRF-CEM-GFP, KG-1a-GFP, Jurkat-CD7-PEBL, CCRF-CEM-CD7-PEBL, and KG-1a-CD7-PEBL cells, empty GFP and an ER/Golgi retention sequence CD7 antibody lentiviral vector were used for transduction. Flow sorting equipment (Agilent Technologies, Santa Clara, CA, USA) was used to obtain pure Jurkat-GFP, CCRF-CEM-GFP, KG-1a-GFP cells, Jurkat-CD7-PEBL, CCRF-CEM-CD7-PEBL, and KG-1a-CD7-PEBL cell lines.

4.3. Flow cytometry, cell sorting, and antibodies

Cells in the logarithmic growth phase were incubated with the flow cytometry antibodies in PBS containing 1% FBS and incubated for 30 min at 4 °C. A flow cytometer (Beckman, Brea, CA, USA) was used to quantify the phenotype. The following antibodies were

used to analyze the phenotype of cells: anti-CD3-PE (clone HIT3a), anti-CD4-APC (clone RPA-T4), anti-CD8-APC (clone SK1), anti-CD7-APC (clone M-T701), anti-CD25-APC (clone 2A3), anti-CD69-APC (clone L78), anti-CD34-APC (clone 581), anti-CD45-APC (clone HI30), anti-PD-1-APC (clone J43), anti-CCR7-FITC (clone 3D12), anti-CD45RA-APC (clone 5H9), and anti-CD7-PE (clone M-T701) (all from BD Biosciences, Franklin Lakes, NJ, USA) and anti-ITGB1-PE-cy7 (clone TS2/16) and anti-ITGB3-PE-cy7 (clone VI-PL2) (both from BioLegend, San Diego, CA, USA). Effector cells (CD45RA⁺ CCR7⁻), naïve (CD45RA⁺ CCR7⁺), central memory T cells (CD45RA⁻ CCR7⁺), and effector memory T cells (CD45RA⁻ CCR7⁻) were evaluated.

Bone marrow cells from 8-, 4-, and 12-week-old mice were collected from the mice bone marrow by washing with PBS, and the flow cytometry antibodies were incubated with the samples in PBS containing 1% FBS for 30 min at 4 °C. A flow cytometer (Beckman) was used to analyze the cell phenotypes with the following antibodies: anti-Lin-BV421 (clone 17A2), anti-Sca1-PE-cy7 (clone D7), anti-Kit-BV510 (clone ACK2), anti-CD48-FITC (clone HM48-1), anti-CD150-PE (clone TC15-12F12.2), anti-CD34-APC-cy7 (clone HM34), anti-IL-7R α -FITC (clone A7R34), and anti-CD16/32-APC (clone 93) (all from BioLegend). HSC (LSK CD150⁺ CD48⁻), LT-HSC (LSK CD150⁺ CD48⁻ CD34⁻), ST-HSC (LSK CD150⁺ CD48⁻ CD34⁺), MPP (LSK CD150⁻ CD48⁻), HPC-1 (LSK CD150⁻ CD48⁺), HPC-2 (LSK CD150⁺ CD48⁺), CLP (LS^{int}K^{int}IL-7R⁺), CMP (LS⁻K⁻IL-7R α ⁻ CD16/32⁻ CD34⁺), GMP (LS⁻K⁻IL-7R⁻ CD16/32⁺ CD34⁺), MEP (LS⁻K⁻IL-7R α ⁻ CD16/32⁻ CD34⁻) were evaluated.

The mice thymus, spleen, lung, liver, and kidney were removed and ground through a 75- μ m filter. The cells were incubated with flow cytometry antibodies in PBS containing 1% FBS and incubated at 4 °C for 30 min. A flow cytometer (Beckman) was used to analyze the cell phenotype using the following antibodies: anti-CD45R-PE-cy5 (clone RA3-6B2), anti-CD4-FITC (clone GK1.5), anti-CD8a-BV421 (clone 53-6.7), anti-CD25-PE-cy7 (clone 3C7), anti-CD44-PE (clone IM7), anti-TCR-APC-cy7 (clone H57-597), anti-CD3 ϵ -PE (clone 145-2C11), anti-CD19-PE-cy7 (clone 6D5), anti-CD11c-FITC (clone N418), anti-NK1.1-FITC (clone S17016D), anti-Gr-1-PE (clone RB6-8C5), anti-F4/80-PE-cy7 (clone BM8), anti-CD11b-FITC (clone M1/70), anti-CD36-APC (clone HM36), anti-IFN- γ -APC (clone XMG1.2), anti-IL-4-PE-cy7 (clone 11B11), anti-IL-17A-PE (clone TC11-18H10.1), anti-FOXP3-PE (clone 150D), anti-CD4-FITC (clone RM4-5), and anti-CD36-APC (clone HM36) (all from BioLegend). DN1 (CD45R⁻ CD4⁻ CD8⁻ CD25⁻ CD44⁺), DN2 (CD45R⁻ CD4⁻ CD8⁻ CD25⁺ CD44⁺), DN3 (CD45R⁻ CD4⁻ CD8⁻ CD25⁺ CD44⁻), DN4 (CD45R⁻ CD4⁻ CD8⁻ CD25⁻ CD44⁻), ISP (CD45R⁻ CD4⁻ CD8⁺ TCR⁻), DP (CD45R⁻ CD4⁺ CD8⁺), SP4 (CD45R⁻ CD4⁺ CD8⁻), SP8 (CD45R⁻ CD4⁻ CD8⁺), B cells (CD3⁻ CD19⁺), T cells (CD3⁺ CD19⁻), NK cells (CD3⁻ NK1.1⁺), NKT cells (CD3⁺ NK1.1⁺), Dendritic cells (CD3⁻ CD11c⁺), Granulocytes (Gr-1⁺), Monocytes (Gr-1⁻ F4/80⁻ CD11b⁺), Macrophages (Gr-1⁻ F4/80⁺ CD11b⁺), Th1 (CD4⁺ IFN- γ ⁺), Th2 (CD4⁺ IL-4⁺), Th17 (CD4⁺ IL-17A⁺), Treg (CD4⁺ Foxp3⁺), were evaluated.

To sort CD8⁺ T cells from the mice spleen, the mice spleen was aseptically removed, ground on a 75- μ m filter, and the cells were incubated in PBS containing anti-CD8b-FITC (clone 53-5.8, BioLegend). After incubation for 30 min at 4 °C, CD8⁺ T cells were obtained using a flow sorting instrument (BD Biosciences), and the cells were used for functional analysis.

4.4. Detection of cell apoptosis and cycle

Cells in the logarithmic growth phase were used to detect apoptosis with an Annexin V-APC 7AAD apoptosis kit (MultiSciences Biotech, Hangzhou, China). A flow cytometer (Beckman) was used to quantify apoptosis.

For the cell cycle assay, cells in the logarithmic growth phase were selected and washed with PBS. After adding 4% paraformaldehyde (NCM Biotech, Providence, RI, USA) and incubating cells at room temperature for 10 min, cells were washed with PBS, and Ki67 antibody (clone 11F6, BioLegend) was added for incubation for 30 min at 4 °C. After washing with PBS, 7-AAD (BD Biosciences) was added at 15 min before loading. Flow cytometry (Beckman) was performed to detect and analyze Early apoptotic cells (7-AAD⁻, Annexin V⁺), Late apoptotic cells (7-AAD⁺, Annexin V⁺), G0 phase cells (Ki67⁻, 7-AAD⁻), G1 phase cells (Ki67⁻, 7-AAD⁺), S, G2, and M phase cells (Ki67⁺, 7-AAD⁺).

4.5. Detection of cell adhesion, migration, invasion, and chemotaxis ability

To evaluate the cell adhesion ability, Matrigel (Corning, NY, USA) and serum-free RPMI medium were diluted at a ratio of 1:19 and coated onto a 96-well plate. An appropriate number of cells was added to the coated 96-well plate, followed by incubation at 37 °C 5% CO₂ for 2 h and washing. Next, CCK-8 (Kesaieen, Shanghai, China) was added and incubated at 37 °C for 3 h, and then a microplate reader (Molecular Devices, Sunnyvale, CA, USA) was used to detect the OD450. A larger value indicated stronger adhesion ability.

To evaluate the migration ability of the cells, the cells were starved for one day by culture in 0.5% BSA serum-free RPMI medium for 12 h. On the next day, cells were added to the upper chamber of the transwell (Corning, NY, USA), and an RPMI medium containing 10% FBS was added to the lower chamber. After 3 days, cells in the lower chamber were counted using an automatic fluorescent cell counter (Countstar, Shanghai, China).

To detect cell invasion (infiltration) ability, the cells were starved for one day by culture in 0.5% BSA serum-free RPMI medium for 12 h. On the next day, Matrigel (Corning) and serum-free RPMI medium were diluted at a ratio of 1:7. Diluted Matrigel was coated in the upper chamber of the transwell (Corning), after which cells were added to the upper chamber. The lower chamber was filled with RPMI medium containing 10% FBS. After 3 days, cells in the lower chamber were counted using an automatic fluorescent cell counter (Countstar).

To evaluate the chemotactic ability of the cells, tumor cells inoculated into the lower chamber of the transwell were labeled with CFSE (10 μ M). On the next day, T cells were seeded into the upper chamber of the transwell (Corning). On day 3, all cells were removed from the lower chamber and subjected to flow cytometry (Beckman) to analyze the proportion of negative cells in the FITC channel and determine the number of chemotactic cells.

4.6. Detection of the expansion ability of mice thymus and spleen cells

The spleen and thymus of the mice were removed under aseptic conditions and then ground through a 75- μ m filter. Mice thymocytes were cultured in RPMI medium containing 1 μ g/mL Con A or 1 μ g/mL Con A + 100 U/mL IL-2 to stimulate cell proliferation. The cells were inoculated into a culture medium in a 96-well plate, a CCK-8 kit (Kesaieen) was added, and a microplate reader (Molecular Devices) was used to detect the OD450 nm. Mice spleen cells were first stained with CFSE (10 μ M), and then cultured in RPMI medium containing 1 μ g/mL ConA or 1 μ g/mL ConA + 100 U/mL IL-2. The cells were removed and incubated with anti-CD3e-PE (clone 145-2C11, BioLegend), anti-CD19-PE-cy7 (clone 6D5, BioLegend), and anti-Gr-1-PE (clone RB6-8C5, BioLegend) antibodies in PBS for 30 min at 4 °C. Finally, flow cytometry (Beckman) was performed to analyze the T, B, and granulocytes and detect the average fluorescence intensity using the FITC channel.

4.7. qPCR

An RNA isolation reagent kit (Omega Bio-tek, Inc.) was used to extract total RNA from the cells. Genomic DNA was removed by treatment with DNase, and the RNA was converted to cDNA (Thermo Fisher Scientific). cDNA was used to evaluate RNA expression by qPCR (Applied Biosystems, Foster City, CA, USA), human CXCR4, CCR4, CXCL13, CCR5, AKT1, CD36, ITGAL, ITGA4, ITGA5, ITGAV, ITGB1, ITGB3, ITGB5, ITGB7, CDK6 genes were tested, mice TNF- α , IFN- γ , IL-6, IL-2 genes were tested and calculated using the $\Delta\Delta$ CT method [46]. The primers are shown below. CXCR4-F: ACTACACCGAGAAATGGGCT, CXCR4-R: CCCACAATGCCAGTTAAGAAGA, CCR4-F: CCTTGCCATCTCGGATCTGC, CCR4-R: AGACCTAGCCCAAAAACCCAC, CXCL13-F: GCTTGAGGTGTAGATGTGTCC, CXCL13-R: CCCACGGGGCAAGATTTGAA, CCR5-F: TTGCCAAACGCTTCTGCAAAT, CCR5-R: AGTGGATCGGGTGTAAACTGA, AKT1-F: GTCATCGAACGCACCTTCCAT, AKT1-R: AGCTTCAGTACTCAAACCTCGT, CD36-F: CTTTGGCTTAATGAGACTGGGAC, CD36-R: GCAACAAACATCACCACACCA, ITGAL-F: TGCTTATCATCATCAGGATGG, ITGAL-R: CTCTCCTTGGTCTGAAAATGCT, ITGA4-F: CACAACACGCTGTTCCGCTA, ITGA4-R: CGATCCTGCATCTGTAAATCGC, ITGA5-F: GGCTTCAACTTAGACGCGGAG, ITGA5-R: TGGCTGGTATTAGCCTTGGGT, ITGAV-F: GCTGTCGGAGATTTCATGGT, ITGAV-R: TCTGCTCGCCAGTAAAATTGT, ITGB1-F: CCTACTTCTGCACGATGTGATG, ITGB1-R: CCTTTGCTACGGTTGGTTACATT, ITGB3-F: CATGAAGGATGATCTGTGGAGC, ITGB3-R: AATCCGCAGGTTACTGGTGAG, ITGB5-F: GGAAGTTCGGAACAGAGGGT, ITGB5-R: CTTTCGCCAGCCAATCTTCTC, ITGB7-F: TGGACCTGAGCTACTCCATGA, ITGB7-R: GGTGAAAGCTGAATGGTGACTG, CDK6-F: GCTGACCAGCAGTACGAATG, CDK6-R: GCACACATCAAACAACCTGACC, TNF- α -F: CAGGCGGTGCCTATGTCTC, TNF- α -R: CGATCACCCGAAAGTTCAGTAG, IFN- γ -F: ATGAACGC-TACACTGCATC, IFN- γ -R: CCATCCTTTTGCCAGTTCCTC, IL-6-F: TAGTCTTCTACCCCAATTCC, IL-6-R: TTGGTCTT AGCCACTCCTC, IL-2-F: GTGCTCCTTGTAACAGCG, IL-2-R: GGGGAGTTTCAGGTTCCGTGA.

4.8. Construction and detection of tumor models

Six-to-eight-week-old NCG mice were purchased from GemPharmatech (Nanjing, China). Jurkat-GFP cells (5×10^6) and Jurkat-CD7-PEBL cells (5×10^6) were inoculated into NCG mice via tail vein injection, and the survival period and bodyweight of the mice were tested every 3 days. Peripheral blood samples were collected weekly to test the tumor burden in the peripheral blood, and anti-CD45-APC (clone HI30, BD Biosciences) was used for flow cytometry.

For tumor transplantation experiments, 5×10^4 B16-F10 cells were injected subcutaneously into C57BL/6J mice in 50 μ L PBS. The tumor was measured every 2 days after tumor transplantation or the designated treatment. The tumor volume was calculated as follows: volume = (length \times width 2)/2.

4.9. Detection of anti-B16-F10 specific antibody content in peripheral blood of mice

The peripheral blood of mice inoculated with tumors was collected and centrifuged at 1000 \times g for 30 min to obtain the blood serum of mice. We incubated 10 μ L mice peripheral blood serum with the same number of B16-F10 cells at 4 °C for 30 min, after which anti-mouse IgG Fc-PE (clone RMG1-1, BioLegend) was added and incubated at 4 °C for 30 min, followed by flow cytometry (Beckman). The average fluorescence intensity was measured.

4.10. Generation of CAR-T cells

We constructed a three-generation CAR structure for CD276. Using lentiviral transfection, the CAR structure virus and CD7-PEBL virus were co-transfected into T cells that had been activated by TransAct (Miltenyi Biotec) for two days, and CD276-CAR-T-CD7-PEBL cells were obtained.

4.11. T cells and CAR-T cells killing ability detection

The ability of T cells and CAR-T cells to kill tumor cells was detected using a real-time quantitative cell analyzer (ACEA BIO, Hangzhou, China). First, 1×10^4 tumor cells were inoculated into a 16-well plate; on the next day, according to the effector cell: target cell ratio (E: T), corresponding T cells or CAR-T cells were added, and the normalized cell index was determined within two days.

4.12. Statistical analysis

For all *in vitro* experiments, data were assessed using GraphPad Prism 6 software (GraphPad, Inc., San Diego, CA, USA). Significance was calculated by Student's *t*-test, and all data are presented as the mean \pm SEM as indicated. Mice survival was analyzed using the log-rank (Mantel-Cox) test.

Formatting of funding sources

This work was supported by the Natural Science Foundation of China (Grant No.81872431 and Grant No. 31471283), the National Key R&D Program of China (2016YFC1303403), Priority Academic Program Development of Jiangsu Higher Education Institutions, the Collaborative Innovation Major Project (Grant No. XYXT- 2015304), the Six Talent Peaks Project in Jiangsu Province (No. SWYY-CXTD-010), the Natural Science Foundation of the Jiangsu Higher Education Institutions of China (General Program, Grant No.19KJD320003). This study was supported by the Project of State Key Laboratory of Radiation Medicine and Protection, Soochow University, (No. GNZ1201803), the Key R&D project of Anhui Province: the clinical application research of chimeric antigen receptor modified $\gamma\delta$ T cells (CAR- $\gamma\delta$ T cells) in malignant tumors with recurrent and refractory CD7 positive T cells, project number: 201904a07020102, : .

Author contribution statement

Binjie Sheng: Conceived and designed the experiments; Performed the experiments; Analyzed and interpreted the data; Contributed reagents, materials, analysis tools or data; Wrote the paper.

Kailu Zhang; Shuaiyu Tian; Renyuxue Ma; Zixuan Li; Hai Wu; Tian Wang; Licui Jiang: Performed the experiments.
Fengtao You; Gangli An; Huimin Meng; Lin Yang; Xin Liu: Contributed reagents, materials, analysis tools or data.

Data availability statement

Data included in article/supp. material/referenced in article.

Declaration of competing interest

The authors declare that they have no known competing financial interests or personal relationships that could have appeared to influence the work reported in this paper.

Acknowledgments

We wish to thank Professor Huang Yuhui for providing the B16–F10 cell line. Funding from the Natural Science Foundation of China Foundation is gratefully acknowledged.

Appendix A. Supplementary data

Supplementary data to this article can be found online at <https://doi.org/10.1016/j.heliyon.2023.e16961>.

References

- [1] A. Aruffo, et al., Molecular cloning of two CD7 (T-cell leukemia antigen) cDNAs by a COS cell expression system, *EMBO J.* 6 (11) (1987) 3313–3316.
- [2] H. Rabinowich, et al., Whiteside, Expression and function of CD7 molecule on human natural killer cells, *J. Immunol.* 152 (2) (1994) 517–526.
- [3] U. Reinhold, et al., CD7- T cells represent a subset of normal human blood lymphocytes, *J. Immunol.* 150 (5) (1993) 2081–2089.
- [4] S. Cortelazzo, et al., Lymphoblastic lymphoma, *Crit. Rev. Oncol. Hematol.* 79 (3) (2011) 330–343.
- [5] R.E. Lewis, et al., The immunophenotype of pre-TALL/LBL revisited, *Exp. Mol. Pathol.* 81 (2) (2006) 162–165.
- [6] Y.T. Png, et al., Blockade of CD7 expression in T cells for effective chimeric antigen receptor targeting of T-cell malignancies, *Blood Adv.* 1 (25) (2017) 2348–2360.
- [7] G. Del Poeta, et al., CD7 expression in acute myeloid leukemia, *Leuk. Lymphoma* 17 (1–2) (1995) 111–119.
- [8] H.F. Tien, et al., CD7 positive hematopoietic progenitors and acute myeloid leukemia and other minimally differentiated leukemia, *Leuk. Lymphoma* 31 (1–2) (1998) 93–98.
- [9] S.D. Lyman, et al., Identification of CD7 as a cognate of the human K12 (SECTM1) protein, *J. Biol. Chem.* 275 (5) (2000) 3431–3437.
- [10] K.E. Pace, et al., Restricted receptor segregation into membrane microdomains occurs on human T cells during apoptosis induced by galectin-1, *J. Immunol.* 163 (7) (1999) 3801–3811.
- [11] G.K. Lam, et al., Expression of the CD7 ligand K-12 in human thymic epithelial cells: regulation by IFN-gamma, *J. Clin. Immunol.* 25 (1) (2005) 41–49.
- [12] T. Wang, et al., K12/SECTM1, an interferon- γ regulated molecule, synergizes with CD28 to costimulate human T cell proliferation, *J. Leukoc. Biol.* 91 (3) (2012) 449–459.
- [13] T. Wang, et al., SECTM1 produced by tumor cells attracts human monocytes via CD7-mediated activation of the PI3K pathway, *J. Invest. Dermatol.* 134 (4) (2014) 1108–1118.
- [14] K.E. Pace, et al., CD7 delivers a pro-apoptotic signal during galectin-1-induced T cell death, *J. Immunol.* 165 (5) (2000) 2331–2334.

- [15] B.N. Stillman, et al., Galectin-3 and galectin-1 bind distinct cell surface glycoprotein receptors to induce T cell death, *J. Immunol.* 176 (2) (2006) 778–789.
- [16] H.S. Koh, et al., CD7 expression and galectin-1-induced apoptosis of immature thymocytes are directly regulated by NF-kappaB upon T-cell activation, *Biochem. Biophys. Res. Commun.* 370 (1) (2008) 149–153.
- [17] H. Rabinowich, et al., Signaling via CD7 molecules on human NK cells. Induction of tyrosine phosphorylation and beta 1 integrin-mediated adhesion to fibronectin, *J. Immunol.* 153 (8) (1994) 3504–3513.
- [18] Y. Shimizu, et al., Crosslinking of the T cell-specific accessory molecules CD7 and CD28 modulates T cell adhesion, *J. Exp. Med.* 175 (2) (1992) 577–582.
- [19] T. Kondoh, et al., CD7 promotes extramedullary involvement of the B-cell acute lymphoblastic leukemia line Tanoue by enhancing integrin beta2-dependent cell adhesiveness, *Int. J. Oncol.* 45 (3) (2014) 1073–1081.
- [20] J.A. Ledbetter, et al., Crosslinking of surface antigens causes mobilization of intracellular ionized calcium in T lymphocytes, *Proc. Natl. Acad. Sci. U. S. A.* 84 (5) (1987) 1384–1388.
- [21] S. Carrel, et al., Direct involvement of CD7 (gp40) in activation of TcR gamma/delta⁺ T cells, *Eur. J. Immunol.* 21 (5) (1991) 1195–1200.
- [22] L.K. Jung, et al., CD7 augments T cell proliferation via the interleukin-2 autocrine pathway, *Cell. Immunol.* 141 (1) (1992) 189–199.
- [23] K. Yoshikawa, et al., Isolation and characterization of mouse CD7 cDNA, *Immunogenetics* 37 (2) (1993) 114–119.
- [24] D.M. Lee, et al., Immunologic characterization of CD7-deficient mice, *J. Immunol.* 160 (12) (1998) 5749–5756.
- [25] F.A. Bonilla, et al., Targeted gene disruption of murine CD7, *Int. Immunol.* 9 (12) (1997) 1875–1883.
- [26] G.D. Sempowski, et al., Resistance of CD7-deficient mice to lipopolysaccharide-induced shock syndromes, *J. Exp. Med.* 189 (6) (1999) 1011–1016.
- [27] C.S. Heinly, et al., Comparison of thymocyte development and cytokine production in CD7-deficient, CD28-deficient and CD7/CD28 double-deficient mice, *Int. Immunol.* 13 (2) (2001) 157–166.
- [28] F. You, et al., A novel CD7 chimeric antigen receptor-modified NK-92MI cell line targeting T-cell acute lymphoblastic leukemia, *Am. J. Canc. Res.* 9 (1) (2019) 64–78.
- [29] D. Gomes-Silva, et al., CD7 CAR T cells for the therapy of acute myeloid leukemia, *Mol. Ther.* 27 (1) (2019) 272–280.
- [30] D. Gomes-Silva, et al., CD7-edited T cells expressing a CD7-specific CAR for the therapy of T-cell malignancies, *Blood* 130 (3) (2017) 285–296.
- [31] M.Y. Kim, et al., CD7-deleted hematopoietic stem cells can restore immunity after CAR T cell therapy, *JCI Insight* 6 (16) (2021), e149819.
- [32] L.K. Jung, et al., Defective expression of T cell-associated glycoprotein in severe combined immunodeficiency, *J. Clin. Invest.* 77 (3) (1986) 940–946.
- [33] A.S. Chan, et al., CD7-mediated regulation of integrin adhesiveness on human T cells involves tyrosine phosphorylation-dependent activation of phosphatidylinositol 3-kinase, *J. Immunol.* 159 (2) (1997) 934–942.
- [34] S.G. Ward, et al., Antibody ligation of CD7 leads to association with phosphoinositide 3-kinase and phosphatidylinositol 3,4,5-trisphosphate formation in T lymphocytes, *Eur. J. Immunol.* 25 (2) (1995) 502–507.
- [35] D.M. Lee, et al., Functional association of CD7 with phosphatidylinositol 3-kinase: interaction via a YEDM motif, *Int. Immunol.* 8 (8) (1996) 1195–1203.
- [36] A.S. Chan, et al., Tyrosine kinase activity associated with the CD7 antigen: correlation with regulation of T cell integrin function, *Eur. J. Immunol.* 24 (11) (1994) 2602–2608.
- [37] T. Fukumori, et al., CD29 and CD7 mediate galectin-3-induced type II T-cell apoptosis, *Cancer Res.* 63 (23) (2003) 8302–8311.
- [38] M.H. Ginsberg, Integrin activation, *BMB Rep.* 47 (12) (2014 Dec) 655–659.
- [39] R.E. Ware, et al., T cell CD7 mRNA expression is regulated by both transcriptional and post-transcriptional mechanisms, *Int. Immunol.* 5 (2) (1993) 179–187.
- [40] M. Rincón, et al., Cyclic AMP and calcium regulate at a transcriptional level the expression of the CD7 leukocyte differentiation antigen, *J. Biol. Chem.* 267 (25) (1992) 18026–18031.
- [41] A.I. Lazarovits, et al., CD7 is associated with CD3 and CD45 on human T cells, *J. Immunol.* 153 (9) (1994) 3956–3966.
- [42] Y. Shu, et al., M2 polarization of tumor-associated macrophages is dependent on integrin beta3 via peroxisome proliferator-activated receptor-gamma up-regulation in breast cancer, *Immunology* 160 (4) (2020) 345–356.
- [43] Y. Zhang, et al., Convallatoxin promotes M2 macrophage polarization to attenuate atherosclerosis through PPAR-gamma-integrin alpha5beta5 signaling pathway, *Drug Des. Dev. Ther.* 15 (2021) 803–812.
- [44] S. Fu, et al., Impaired lipid biosynthesis hinders anti-tumor efficacy of intratumoral iNKT cells, *Nat. Commun.* 11 (1) (2020) 438.
- [45] H. Wang, et al., CD36-mediated metabolic adaptation supports regulatory T cell survival and function in tumors, *Nat. Immunol.* 21 (3) (2020) 298–308.
- [46] K.J. Livak, et al., Analysis of relative gene expression data using real-time quantitative PCR and the 2(-Delta Delta C(T)) Method, *Methods* (2001) 402–408.